

Oil & Natural Gas Technology

DOE Award No.: DE-FE0028895

Quarterly Research Performance

Progress Report (Period Ending 12/31/2018)

Dynamic Behavior of Natural Seep Vents: Analysis of Field and Laboratory Observations and Modeling

Project Period (10/01/2016 to 09/30/2019)

Submitted by:
Scott A. Socolofsky



Signature

Texas A&M Engineering Experiment Station
DUNS #:847205572
3136 TAMU
College Station, TX 77843-3136
Email: socolofs@tamu.edu
Phone number: (979) 845-4517

Prepared for:
United States Department of Energy
National Energy Technology Laboratory

Submitted 01/31/2019



U.S. DEPARTMENT OF
ENERGY



NATIONAL
ENERGY
TECHNOLOGY
LABORATORY

Office of Fossil Energy

DISCLAIMER:

This report was prepared as an account of work sponsored by an agency of the United States Government. Neither the United States Government nor any agency thereof, nor any of their employees, makes any warranty, express or implied, or assumes any legal liability or responsibility for the accuracy, completeness, or usefulness of any information, apparatus, product, or process disclosed, or represents that its use would not infringe privately owned rights. Reference herein to any specific commercial product, process, or service by trade name, trademark, manufacturer, or otherwise does not necessarily constitute or imply its endorsement, recommendation, or favoring by the United States Government or any agency thereof. The views and opinions of authors expressed herein do not necessarily state or reflect those of the United States Government or any agency thereof.

Contents

1 Accomplishments	8
1.1 Summary of Progress Toward Project Objectives	8
1.2 Progress on Research Tasks	9
1.2.1 Task 1.0: Project Management Planning	9
1.2.2 Task 2.0: Analyze NETL Water Tunnel Data	9
1.2.3 Task 3.0: Synthesize GISR Field Data	12
1.2.4 Decision Point 1	13
1.2.5 Task 4.0: Refine and Validate Seep Model	13
1.3 Decision Point 2	31
1.3.1 Task 5.0: Conduct No-Hydrate M3 Calibration Experiment in OTRC	32
1.3.2 Task 6.0: Apply Seep Model to GISR Multibeam Echosounder Data	32
1.3.3 Task 7.0: Document Model Validation	33
1.4 Deliverables	33
1.5 Milestones Log	34
1.6 Plans for the Next Reporting Period	34
2 Products	38
2.1 Publications, Conference Papers, and Presentations	38
2.2 Websites or Other Internet Sites	38
2.3 Technologies or Techniques	38
2.4 Inventions, Patent Applications, and/or Licenses	38
2.5 Other Products	38
3 Participants and other collaborating organizations	38
3.1 Project Personnel	38
3.2 Partner Organizations	40
3.3 External Collaborators or Contacts	40
4 Impact	40
5 Changes / Problems	40

6	Special Reporting Requirements	41
7	Budgetary Information	41

List of Figures

1	Project Timeline.	10
2	Comparison of observed and modeled mass transfer rate dm/dt for pure methane bubbles in RO water considering only experiments that do not form a hydrate shell.	17
3	Comparison of observed and modeled mass transfer rate dm/dt for natural gas mixture bubbles (C1C2C3) in RO water considering only experiments that do not form a hydrate shell.	18
4	Comparison of observed and modeled mass transfer rate dm/dt for natural gas mixture bubbles (C1C2C3) in artificial seawater considering only experiments that do not form a hydrate shell.	19
5	Comparison of observed and modeled mass transfer rate dm/dt for natural gas mixture bubbles (C1C2C3) in artificial seawater plus dispersant considering only experiments that do not form a hydrate shell.	19
6	Comparison of TAMOC model simulations with the measured data. Upper panel: equivalent spherical radius; lower panel: bubble mass. Results for a pure methane bubble in RO water.	21
7	Comparison of TAMOC model simulations with the measured data. Upper panel: equivalent spherical radius; lower panel: bubble mass. Results for a natural gas bubble (C1C2C3) in artificial seawater water.	22
8	Bubble properties as a function of time for the natural gas bubble (C1C2C3) presented in Figure 7. Bubble density and rise velocity are computed in TAMOC using the mixture equation of state and tracking the evolving mixture as the bubble dissolves. Equivalent parameters are computed in the NETL report data assuming a constant bubble composition.	23
9	Comparison of observed and modeled mass transfer rate dm/dt for pure methane bubbles in RO water with a hydrate skin.	25
10	Comparison of TAMOC model simulations with the measured data. Upper panel: equivalent spherical radius; lower panel: bubble mass. Results for a pure methane bubble in RO water with a hydrate skin at $T_{hyd} < 10^{\circ}\text{C}$	26

11 Comparison of TAMOC model simulations with the measured data: equivalent spherical radius. Results for a pure methane bubble in RO water for an experiment with variable system pressure. Upper panel: low pressure experiment; lower panel: high-pressure experiment. 27

12 Comparison of TAMOC model simulations with the measured data: equivalent spherical radius. Results for a pure methane bubble in RO water for an experiment with constant pressure at $T_{hyd} > 10^{\circ}\text{C}$. Modeled using C_s of hydrate instead of free gas. 27

List of Tables

1	Values of the mass transfer correlation parameter α in the NETL HPWT experimental dataset.	20
2	Milestones schedule and verification methods.	35
3	Budget Report for Phase 1	42
4	Budget Report for Phase 2	43
5	Budget Report for Phase 3	44

1 Accomplishments

1.1 Summary of Progress Toward Project Objectives

The *overarching goal* of this project is to develop a computer model to predict the trajectory and dissolution of hydrate-armored methane bubbles originating from natural seeps. The model is based on the Texas A&M Oilspill (Outfall) Calculator (TAMOC), developed by Dr. Socolofsky, and which will be refined and validated through this project to explain fundamental laboratory and field observation of methane bubbles within the gas hydrate stability zone of the ocean water column. *Our approach* is to synthesize fundamental observations from the National Energy Technology Laboratory's (NETL) High-Pressure Water Tunnel (HPWT) and field observations from the Gulf Integrated Spill Research (GISR) seep cruises (cruises G07 and G08), conducted by the PIs in the Gulf of Mexico, to determine the dissolution pathways and mass transfer rates of natural gas bubbles dissolving in the deep ocean water column. We will achieve these objectives by pursuing the *following specific objectives*:

1. Analyze existing data from the NETL HPWT.
2. Synthesize data from the GISR natural seep cruises.
3. Refine and validate the seep model to predict available data.
4. Demonstrate the capability of the seep model to interpret multibeam data.

Ultimately, the *main outcome and benefit* of this work will be to clarify the processes by which hydrate-coated methane bubbles rise and dissolve into the ocean water column, which is important to predict the fate of methane in the water column, to understand the global carbon cycle, and to understand how gas hydrate deposits are maintained and evolve within geologic and oceanic systems, both at present baselines and under climate-driven warming.

During this reporting period, we focused on Tasks 4 and 6 and began Task 7. For the seep model validation (Task 4), we have applied our model to simulate each of the experiments conducted in the NETL HPWT. These simulations take two forms. First, we compute the mass reduction rate predicted by the model at the initial thermodynamic conditions of each experiment and compare this to the measured, average bubble shrinkage rates. This provides a validation of the mass transfer rates in the model, and demonstrates that the bubbles in the NETL HPWT dissolve about 1.6 times faster than bubbles in quiescent water. Second, we simulate the dynamic bubble sizes for

each experiment. In this activity, we simulate the mean mass transfer rate and a high and low value spanning 95% of the measured values. This demonstrates the sensitivity of the model results to the mass transfer rate and allows us to quantify the model performance. The complete set of model results is archived in a data directory, and this data satisfies Milestone 5: Quantify seep model performance. We have also continued to apply our seep model to evaluate the GISR multibeam data (Task 6), in particular focusing on the EM-302 watercolumn data (Task 6.2). Because the filter pump in the Offshore Technology Research Center (OTRC) failed and needed to be replaced, we have had to delay the no-hydrate experiment (Task 5); the laboratory repairs are completed, and this experiment is now scheduled for the next project quarter (February 2019). Finally, we have begun drafting journal papers that summarize our simulation results, a major element of Task 7 (document model validation). A detailed report of our progress on each of these tasks for the present performance period is reported herein.

1.2 Progress on Research Tasks

Figure 1 presents the project timeline, showing each of the project tasks, subtasks, and milestones as identified in the Project Management Plan (PMP), and updated to show Task 5.0 now in the second quarter of Phase 3. The present reporting period concludes the first quarter of FY 2019 (Phase 3 of the project). During this period, we completed work on Task 4, continued effort on Subtask 6.2, and began work on Task 7. The summary of the completed work together with work conducted on these ongoing tasks during the present reporting period is summarized in the following sections.

1.2.1 Task 1.0: Project Management Planning

The Project Management Plan was completed during the first quarter of Phase 1 and accepted in final form as of October 28, 2016.

1.2.2 Task 2.0: Analyze NETL Water Tunnel Data

In this project, we have analyzed the comprehensive data set of HPWT data collected by NETL. To do this, we have transferred a complete copy of all raw data (primarily image files and time history data of pressure and temperature in the HPWT during each experiment) to Texas A&M University and have installed this data on a secure internal server. Data transfer was completed

Task Name	Assigned Resources	Year 1 / Phase 1				Year 2 / Phase 2				Year 3 / Phase 3			
		Qtr 1	Qtr 2	Qtr 3	Qtr 4	Qtr 1	Qtr 2	Qtr 3	Qtr 4	Qtr 1	Qtr 2	Qtr 3	Qtr 4
Task 1.0 - Project Management and Planning	Socolofsky	●											
Task 2.0 - Analyze NETL Water Tunnel Data Subtask 2.1 - Evaluate hydrate formation time Subtask 2.2 - Track hydrate crystals on bubble interface Subtask 2.3 - Validate bubble shrinkage rates Milestone: Obtain NETL HPWT Data Milestone: Adapt Matlab code to NETL data	Socolofsky Socolofsky Wang Wang												
Task 3.0 - Synthesize GISR Field Data Subtask 3.1 - Bubble characteristics from high-speed camera Subtask 3.2 - Synchronize acoustic and camera datasets Milestone: Develop Matlab code for M3 and EM-302 data	Wang Wang Wang												
Decision Point 1													
Task 4.0 - Refine and Validate Seep Model Subtask 4.1 - Validate to NETL Water Tunnel Data Subtask 4.2 - Validate to GISR Field Data Subtask 4.3 - Finalize and distribute seep model Milestone: Adapt seep model to NETL data Milestone: Quantify seep model performance	Socolofsky Socolofsky Socolofsky Socolofsky												
Decision Point 2													
Task 5.0 - Conduct No-Hydrate M3 Experiment Milestone: OTRC Experimental Report	Wang												
Task 6.0 - Apply Seep Model to GISR Multibeam Data Subtask 6.1 - Analyze M3 data to characterize hydrate shells Subtask 6.2 - Analyze EM-302 data for bubble concentration Milestone: Quantify performance of acoustic models	Socolofsky Socolofsky Wang												
Task 7.0 - Document Model Validation Milestone: Complete model validation	Socolofsky												
Task 8.0 - Data Distribution / Archiving	Socolofsky												

Figure 1: Project Timeline.

on March 24, 2017, and achieved Milestone 1 for the project (Obtain NETL HPWT Data). Task 2 was completed as of June 30, 2018. The sections below summarize the key results obtained for each of the Subtasks of this Task.

Subtask 2.1 - Evaluate Hydrate Formation Time

This subtask was completed as of September 30, 2017, and all of the post-processed data has been submitted with the report for Decision Point 1 (see § 1.2.4). In this task, we identified the moment that hydrate skin coverage was completed for each bubble in the experiments as well as for key moments when the hydrate dynamics changed. For a complete description of the data analysis for this subtask and the post-processed results, see the full report for Decision Point 1.

Subtask 2.2 - Track Hydrate Crystals on Bubble Interface

This subtask was completed as of December 31, 2017, and a complete analysis of the results with conclusions was submitted with the first-quarter progress report of FY2018. For this task, we analyzed all of the high-speed camera data for gas bubbles with hydrate shells to track the motion of hydrate plates when the hydrate coverage was not 100%. We found two main types of behavior. First, when hydrate plates are large and their spacing is non-uniform, the plates are observed to translate across the leading edge of the bubbles. The mean speeds of this hydrate shell movement was 10 cm/s, with peak speeds close to the rise velocity of bubbles (20 cm/s). Second, during hydrate dissociation, when many, small hydrate crystals cover the bubble surface in a quasi-uniform distribution, the hydrate particles are not observed to translate over the surface of the bubble. Instead, they remain knitted together, and the boundary condition at the bubble/water interface appears to be no-slip.

Based on these observations, we anticipate that mass transfer rates for the large hydrate shells that move across the leading edge of the bubble will be higher than for dirty bubbles; whereas, we expect the mass transfer rates for hydrate-coated bubbles and cases with small hydrate particles uniformly distributed over the bubble surface to be similar to dirty bubbles or slower. Because the system pressure inside the HPWT was not constant during these events, we will evaluate these mass transfer rates in the context of Task 4 as we compare the model results to these data.

Subtask 2.3 - Validate Bubble Shrinkage Rates

This subtask was completed as of April 30, 2018, and has been reported in several quarterly reports through the project performance period. We adapted our Matlab image analysis program

for bubble size evaluation to the NETL HPWT dataset and compared our results for bubble size to those reported by NETL in their report by Levine et al. (2015). Although there were small differences in our computed sizes, these are attributable to different choices in the cut-off and cut-on criteria for identifying the bubble edge and were negligible in comparison to the inherent variability in the data due to bubble motion. This variability is primarily caused by two factors: 1.) rotation of the bubbles when they have non-spherical shape and 2.) changes in the image magnification as the bubbles move toward and away from the camera. Both factors lead to experimental error in the computed bubble sizes. We evaluated this error by analyzing long data sets in sequentially shorter sample periods. Our analysis concluded that bubble shrinkage rates are converged after a minimum of 500 s of sampling, as this is adequate time for the bubble to wander about the whole measurement volume and experience several rotations. These data will be used extensively in Task 4 as we validate the shrinkage rate predictions of the model to those measured in the HPWT.

Progress Toward Milestones

Milestone 1 (Obtain NETL HPWT Data) was completed on March 24, 2017, and Milestone 2 (Adapt Matlab Code to NETL Data) was completed on September 26, 2017. These Milestones conclude the Milestones associated with Task 2.

1.2.3 Task 3.0: Synthesize GISR Field Data

The project PIs conducted two research cruises to natural seeps in the Gulf of Mexico under funding to the GISR consortium. These were the G07 cruise in July 2014 to Mississippi Canyon (MC) block 118 and to Green Canyon (GC) block 600 and the G08 cruise in April 2015 to MC 118. Both cruises were on the *E/V Nautilus* and utilized the remotely operated vehicle (ROV) *Hercules*. This project utilizes two main datasets from these cruises: data from our stereoscopic high-speed camera system mounted on the ROV (Wang et al. 2015) and acoustic data collected by an M3 sonar mounted on the ROV and an EM-302 multibeam sonar mounted on the haul of the ship. The image data from the G07 cruise was analyzed previously and reported in Wang et al. (2016). This project analyzes all of the acoustic data and performs a complete analysis of the image data for the G08 cruise. This task was completed as of December 2017, and the outcomes of each subtask are reported below.

Subtask 3.1 - Bubble Characteristics from High-Speed Camera.

This subtask was completed as of September 30, 2017, and all of the post-processed data were submitted with the report for Decision Point 1 (see § 1.2.4). In this task, we have analyzed images from our high-speed, stereoscopic image system to compute bubble sizes and the rise velocities of individual bubbles. For a complete description of the data analysis for this subtask and the post-processed results, see the full report for Decision Point 1.

Subtask 3.2 - Synchronize Acoustic and Camera Datasets.

This subtask was completed as of March 31, 2018. Data from the cameras and acoustic measurements have been reported separately. The image data include bubble size distributions and rise velocity, and are reported in the report for Decision Point 1. The acoustic data have been analyzed to predict the *in situ* target strength, which is a measure of the acoustic backscatter from the bubbles within each sample volume. This work was reported in the report for Milestone 3. The final output of this subtask was a calibration curve relating the observed bubble characteristics to the target strength measured by the M3 and EM 302 multibeam sonars. The calibration curve for the EM 302 was reported in our report for Milestone 3, and the calibration curve for the M3 was included in our quarterly report for the second quarter of Phase 2. These data along with results of Task 5 (OTRC experiment) will be used in Task 6 to evaluate the seep model at the field scale.

Progress Toward Milestone

Milestone 3 (Develop Matlab Code for EM 302 and M3 Data) was completed on September 29, 2017. This Milestone concludes the Milestones associated with Task 3.

1.2.4 Decision Point 1

The report for Decision Point 1 was completed and submitted as of October 31, 2017. Based on successful completion of the go/no go success criteria for Decision Point 1 outlined in the PMP, we were granted permission to continue into project Phase 2 and begin work on Task 4.

1.2.5 Task 4.0: Refine and Validate Seep Model

Since the Deepwater Horizon accident, the project PIs have been developing a numerical model to predict the fate of petroleum bubbles and droplets in the ocean water column. This model is called the Texas A&M Oil spill Calculator (TAMOC), and is freely available through <https://github.com/socolofs/tamoc>. This model can compute the dissolution of a natural gas bubble

in the ocean water column, and prior to this project, had been applied to study the fate of methane released from natural gas seeps along the continental slope of the Gulf of Mexico. In this project, we apply this numerical model to simulate the experiments in the NETL High-Pressure Water Tunnel (HPWT; see Task 2) and the field observations from the GISR expeditions (see Task 3). These simulations are used to validate our model for the formation time of hydrate skins of natural gas bubbles within the hydrate stability zone of the oceans and our equations for mass transfer from bubbles with and without a hydrate skin. This model is important to predict the distribution of methane in the ocean water column from natural seeps, accidental oil well blowouts, hydrate production, or from gas release caused by anthropogenic or changing climate forcing.

Subtask 4.1 - Validate to NETL Water Tunnel Data.

In the NETL HPWT experiments, cameras observed the bubbles over time as they dissolved into the surrounding flow, and these experiments were conducted at different pressure and temperature conditions. Because the pressure and temperature in the HPWT is prescribed by the operator and independent of bubble position (the pressure is controlled by a set of piston pumps and the bubble is held at a constant depth in the water tunnel), we have adapted the TAMOC model to allow pressure and temperature to be prescribed functions of time so that we can model the exact conditions experienced by a bubble during an experiment.

As the raw experimental observations are camera images of bubbles, the quantitative observations are obtained by additional image processing and calculations (completed during Task 2 of this project). We identified three sets of derived data values to use in model validation. These are:

1. Hydrate Formation Time. From the bubble images themselves, it is evident whether or not a hydrate shell has formed. We use this information with the experimental timing conditions to determine how long under each thermodynamic state (e.g., temperature, pressure, and background natural gas concentration) it takes for hydrate to form. This yields the transition time for hydrate formation t_{trans} .
2. Mass Transfer Rate. Using an equation of state for density of the gas, we can convert the observed bubble size to bubble mass. From the time series of bubble mass, we can compute the mass loss rate dm/dt . This loss rate relates directly to the mass transfer coefficient β .
3. Bubble Evolution. Image processing of the camera images allows calculation of the equivalent spherical volume of the bubble in each camera frame. This yields time series of equivalent

spherical radius $r_e(t)$ (or diameter $d_e(t)$).

These are the available laboratory data for model validation. Each of the sections below summarizes our usage of this data to validate the TAMOC model predictions.

Validation for Hydrate Transition Time. Our observations of natural seep bubbles in the oceans (i.e., the GISR expeditions, see Task 3 above) suggest that bubbles dissolve quickly when they are first released from the seafloor, matching mass transfer rates for clean bubbles. After a hydrate transition time, the bubble-water interface becomes coated with hydrates, and the mass transfer rates reduce, matching those for dirty bubbles. When simulating natural seeps, we have used correlations for this hydrate transition time to select appropriate mass transfer rates in our model for the pre- and post-hydrate formation phases of the bubble transport.

In the literature for bubbles and droplets (Clift et al. 1978), it is well known that it is very difficult to produce clean bubble mass transfer rates in a laboratory setting. Indeed, this is one reason it is quite surprising to observe clean bubble mass transfer rates in the oceans. As we analyzed the mass transfer rates in the NETL experiments (see next section), we confirmed that the mass transfer rates without a hydrate shell are slightly faster than those for dirty bubbles, but they are much slower than those for clean bubbles. As a result, we should not use clean bubble mass transfer rates to simulate the HPWT experiments. This also means that we should set the hydrate formation time to zero in the TAMOC model when simulating the HPWT data so that dirty bubble mass transfer rates will *always be used*. We can then adjust the theoretical value of the mass transfer rate β for a dirty bubble to those observed in the NETL experiments β_{obs} using a correction factor α following:

$$\beta_{obs} = \alpha\beta \tag{1}$$

We calibrate α in the next section and use the resulting prediction for β_{obs} throughout each HPWT experiment simulation.

We have quantified the time at which hydrate first covers the bubble for each of the experiments in the NETL HPWT dataset that include hydrate and reported these results in Task 2. Our original intent in Subtask 4.1 was to predict this hydrate formation time by correlating to bubble size and hydrate sub-cooling, which is how we solved this problems for hydrated bubbles released in the ocean and at natural seeps. However, the hydrate formation times in the HPWT experiments also depend heavily on the way bubbles were introduced into the water tunnel. Gas was pumped

slowly into an inverted cup while the HPWT was maintained at a pressure just below the hydrate formation point. This time was quite variable, lasting from seconds to several minutes. The pressure was then quickly ramped up to a constant, experimental pressure inside the hydrate stability zone, and the bubble was released. Our data from the field and data from laboratory experiments at low pressure reported in the literature suggest that the transition time from clean to dirty mass transfer rates should depend on the total time the gas was in the water, including the time the gas was accumulating in the cup as surfactants are being scavenged by the gas from the water during this time. This also affects the rate as which hydrates form. Hence, while we have validated that our previous equation for hydrate formation time does predict the hydrates to form at or before the observed times, a direct validation is impossible due to the highly variable gas injection times which depended on the experimental operations and do not correlate with any physical or thermodynamic variables.

As explained above, our model for mass transfer with a hydrate shell assumes dirty bubble mass transfer rates. The mass transfer rates in the NETL HPWT also agree with dirty bubble mass transfer rates for all bubbles at all times (whether with a hydrate shell or not), such that the formation time for hydrate is not needed. A few experiments conducted with high background gas concentration and constant pressure, however, have slower mass transfer rates caused by the hydrate shell. Yet, in these cases, the hydrate formation time is also not needed as the model can be initialized at the moment the hydrate shell has formed. Hence, the formation time for hydrates is not needed to validate the TAMOC model to the present HPWT dataset. In the next paragraphs, we present our analysis of α and quantify the model performance through comparison to the NETL experimental observations.

Validation for Mass Transfer Coefficient. As we have discussed in previous reports, the correct parameter to compare between the model and the measured data with respect to the mass transfer rate is the mass loss rate dm/dt . In this Subtask, we have analyzed the mass loss rates for each of several classes of experiments and evaluated the model performance relative to the measured data. We identify four different classes of experiments, including pure methane bubbles (CH_4) in reverse osmosis (RO) water and methane-ethane-propane mixture bubbles (C1C2C3) in RO water, artificial seawater, and seawater plus dispersant. Each of the experiments conducted within these classes yielded results for bubbles that formed hydrate shells and that did not form hydrate shells.

To determine the parameter α , we evaluate only experiments that did not form hydrate shells as these should agree with theoretical values for mass transfer rate.

Figure 2 compares the measured mass reduction rates dm/dt observed in the HPWT to the model predictions at the experimental initial conditions using dirty bubble mass transfer rates for pure methane bubbles in reverse osmosis (RO) water. These experiments give the baseline

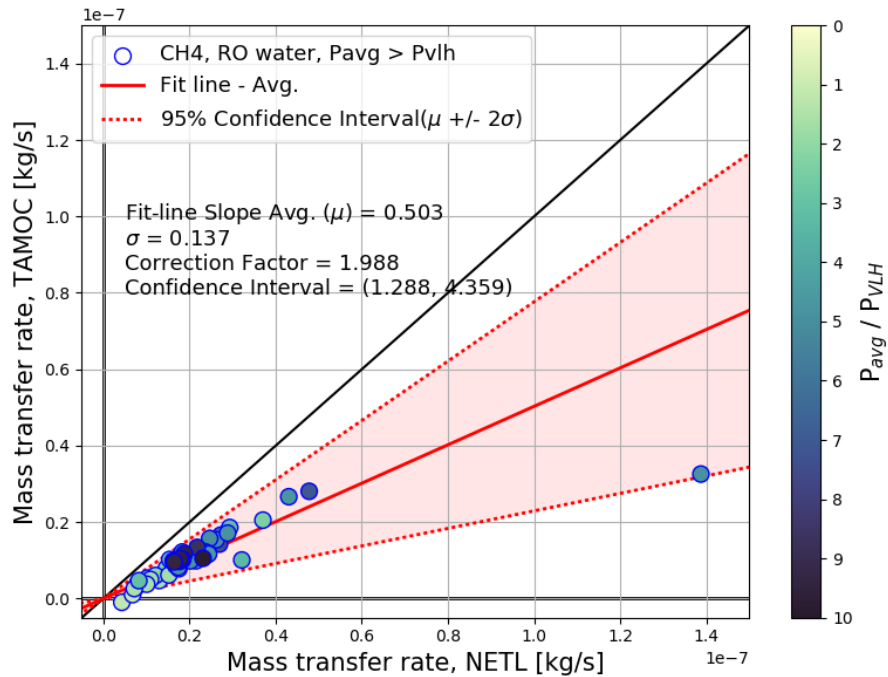


Figure 2: Comparison of observed and modeled mass transfer rate dm/dt for pure methane bubbles in RO water considering only experiments that do not form a hydrate shell.

performance of the HPWT as these data are the closest to the theoretical conditions that are the basis for the TAMOC predictions. The black line in the figure shows the 45° agreement line. Each of the ordered pairs fall below the line, indicating that mass transfer in the HPWT is faster than for a bubble in a quiescent tank. This makes sense because the turbulence in the counterflow of the water tunnel would be expected to increase the mass transfer rates. The best-fit to the experimental observations predicts $\alpha = 1.99$. Also shown in the figure is the 95% confidence limit, which spans $1.29 \leq \alpha \leq 4.36$. Each of the observations is colored by the HPWT pressure P_{avg} relative to the pressure at which hydrate forms P_{VLH} ; many of the observations are made well inside the hydrate stability zone. For these high-pressure experiments, hydrate did not form because the background dissolved gas concentration was low.

We performed similar analyses of the observed and predicted mass transfer rates for the gas

mixture bubbles (C1C2C3) in RO water, artificial seawater, and artificial seawater plus dispersant. Figures 3 to 5 present the results. While these experiments should also be close to the theoretical

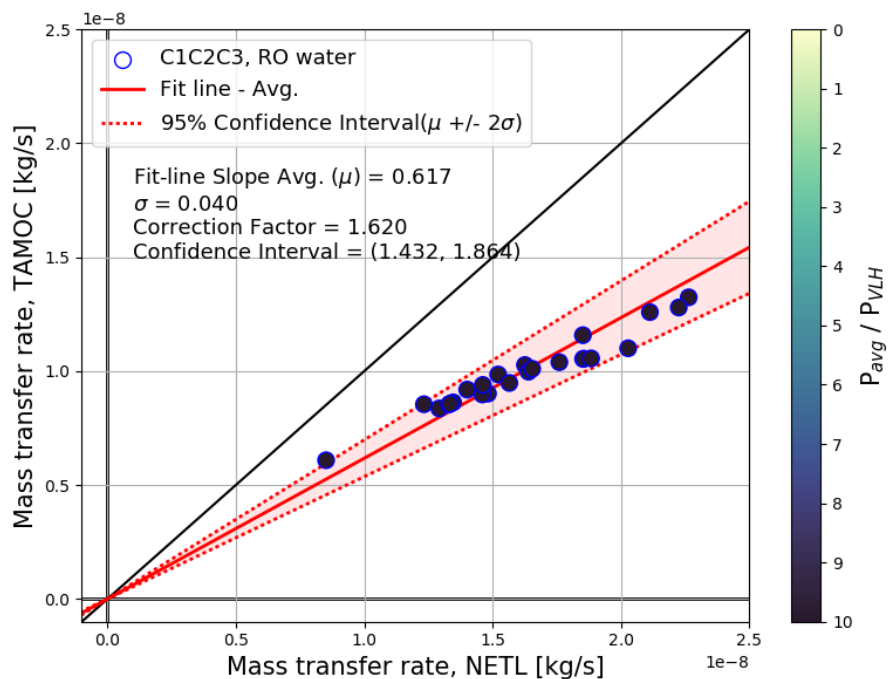


Figure 3: Comparison of observed and modeled mass transfer rate dm/dt for natural gas mixture bubbles (C1C2C3) in RO water considering only experiments that do not form a hydrate shell.

value, because the composition of the bubble is continuously changing throughout the experiment, we would expect greater variability between the average observed mass loss rate and the rate predicted by the model at the experimental initial conditions. The mean values of α range from 1.27 to 1.62, with the 95% confidence limits spanning 1.04 to 1.96. These are slightly lower than the fit in the pure methane case, however, that case is strongly influenced by the single experiment at very high mass transfer rate ($1.4 \cdot 10^{-7}$ kg/s), which is about an order of magnitude greater than the other measured rates. Because the experiments with natural gas mixtures span a lower range of mass loss rates, the data actually have less scatter. Table 1 summarizes all results for evaluation of α .

Our conclusion from this analysis is that the NETL HPWT performs very consistently over a wide range of gas types, background water types, dissolved gas concentration, pressure, and bubble sizes. The average value of the mass transfer amplification factor α is 1.61 with a standard deviation of 0.30. The 95% confidence interval for α is much broader, with mean values spanning 1.3 to 2.5. To understand the importance of this variability, we conduct each validation experiment using

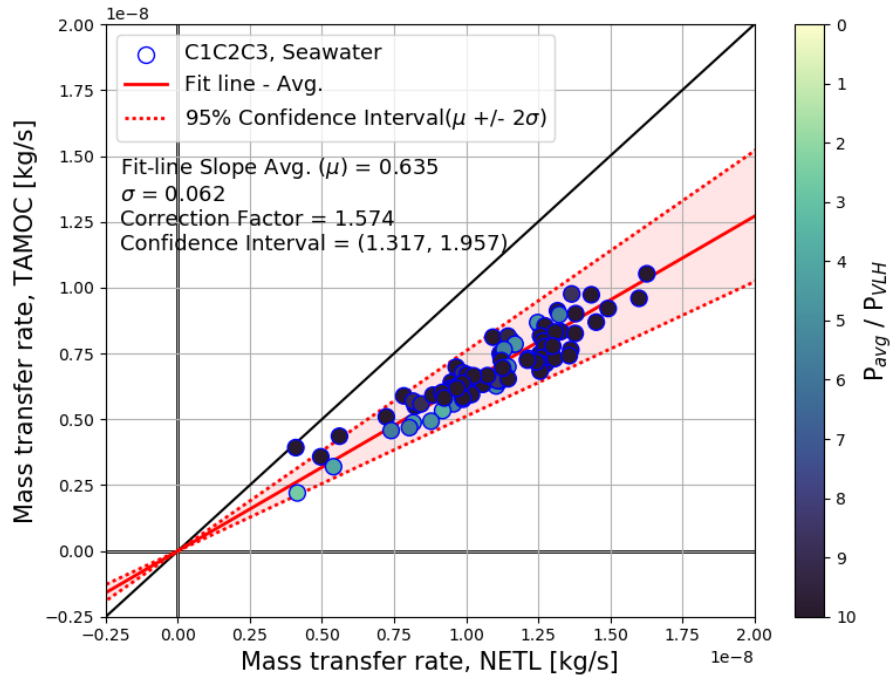


Figure 4: Comparison of observed and modeled mass transfer rate dm/dt for natural gas mixture bubbles (C1C2C3) in artificial seawater considering only experiments that do not form a hydrate shell.

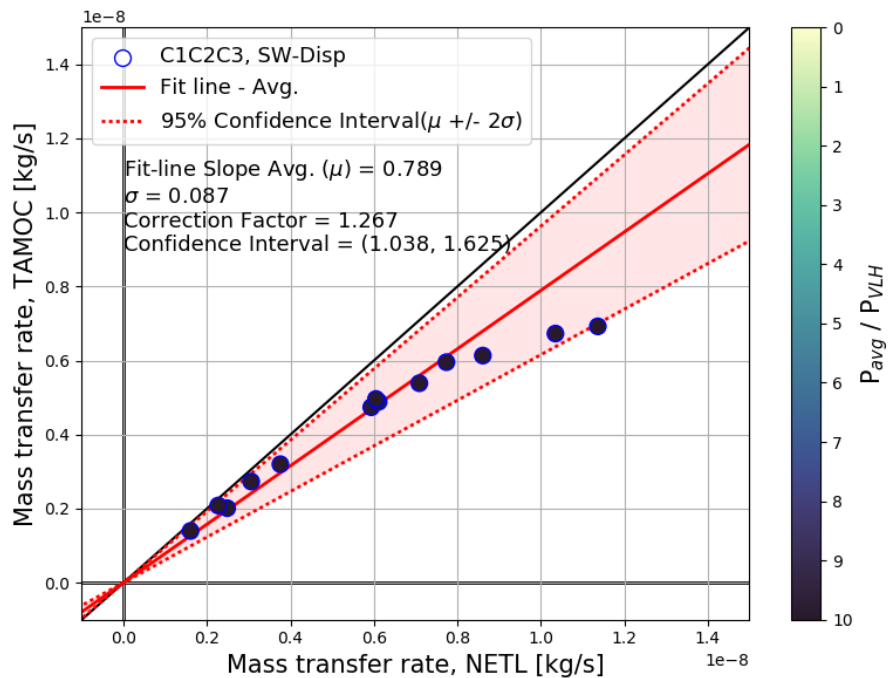


Figure 5: Comparison of observed and modeled mass transfer rate dm/dt for natural gas mixture bubbles (C1C2C3) in artificial seawater plus dispersant considering only experiments that do not form a hydrate shell.

Table 1: Values of the mass transfer correlation parameter α in the NETL HPWT experimental dataset.

Gas	Water	Hydrate	α_{avg}	α_{low}	α_{high}
CH4	RO	No	1.99	1.29	4.36
C1C2C3	RO	No	1.62	1.43	1.86
C1C2C3	Seawater	No	1.57	1.32	1.96
C1C2C3	Seawater + Dispersant	No	1.27	1.04	1.63
Average			1.61	1.27	2.46
Standard Deviation			0.30	0.16	1.27

the mean value of α and the high and low values spanning the 95% confidence interval. These are compared to the measured bubble sizes so that the model performance can be quantified in the next paragraphs.

Validation to Bubble Shrinkage Rate. We have used TAMOC to simulate all of the experimental data in the NETL HPWT dataset. These data are archived in a data repository and will be provided to NETL as part of Milestone 5: Quantify seep model performance. Here, we highlight a few typical results to demonstrate the model performance and explain how to read the archived data.

Cases without Hydrate Formation. For each experiment simulation, we use the calibrated values of α from the analysis above and present the mean model behavior and model simulations with α spanning the 95% confidence limit. Figure 6 presents simulation results for a typical case of a pure methane bubble in RO water without hydrate formation. The dark blue line in the figure reports

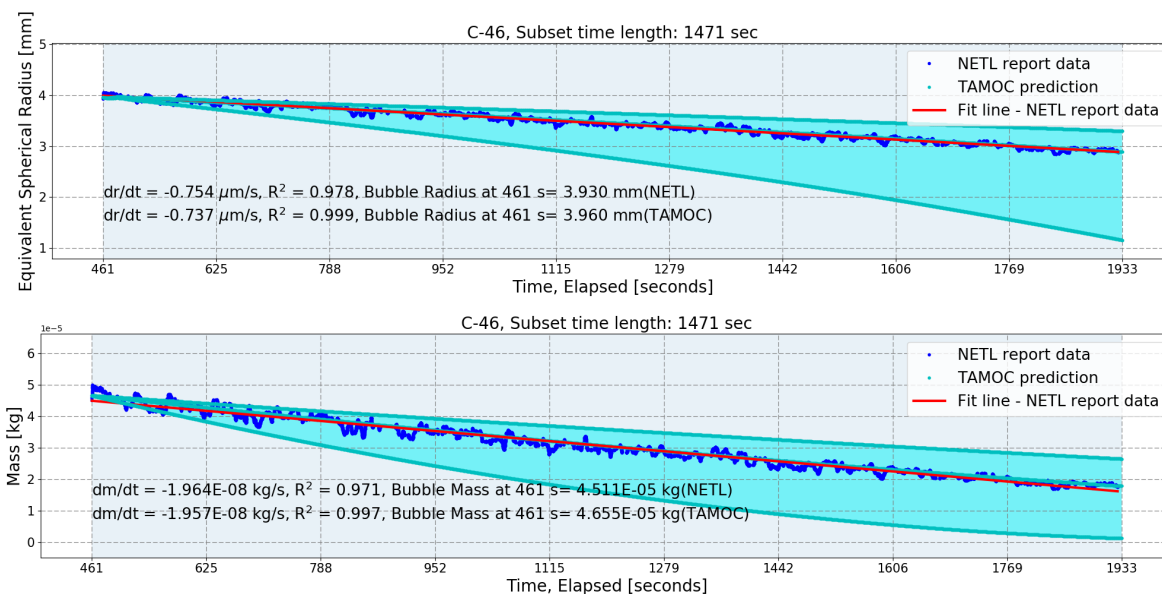


Figure 6: Comparison of TAMOC model simulations with the measured data. Upper panel: equivalent spherical radius; lower panel: bubble mass. Results for a pure methane bubble in RO water.

the measured bubble size (upper panel) and the computed bubble mass (lower panel) using an equation of state for methane. The red line shows the best fit to the measured data as reported previously by Levine et al. (2015). The dark cyan lines present the TAMOC simulate results for the average value of α and for the 95% confidence value of α , with the region between the simulations using the low and high values of α shaded light cyan. For the case in Figure 6, the TAMOC

simulation using the average value of α agrees very well with the measured data, and nearly all of the measurements are within the 95% confidence limit simulations.

Figure 7 presents similar results for a natural gas bubble (C1C2C3) in RO water without hydrate formation. In the upper panel, the TAMOC simulation tracks the measured bubble size very well

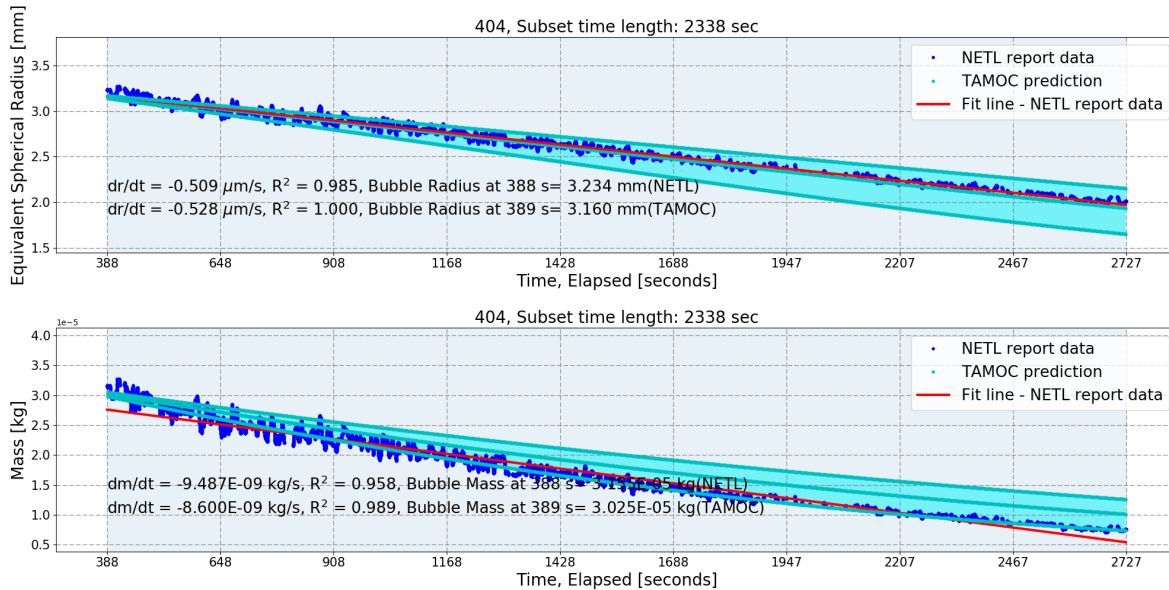


Figure 7: Comparison of TAMOC model simulations with the measured data. Upper panel: equivalent spherical radius; lower panel: bubble mass. Results for a natural gas bubble (C1C2C3) in artificial seawater water.

for the average value of α , and the 95% confidence limit captures most of the data. In the lower panel, the TAMOC simulation is drifting above the results reported in Levine et al. (2015). This can be explained by considering the dissolution. This natural gas bubble contains methane, ethane, and propane. The methane is the most soluble and the first to dissolve. As the methane dissolves, the mole fractions of ethane and propane become larger, and the bubble density increases. TAMOC simulates the accurate removal of methane and subsequent apparent concentration of ethane and propane in the bubble. The equation of state in TAMOC takes this evolving bubble composition into account to compute the bubble mass. As methane dissolves away, the bubble mass increases. The data for mass computed by Levine et al. (2015) assume a constant bubble composition, and hence, lower mass for the same sized bubble.

The difference between assuming a constant bubble composition and using the evolving composition for natural gas as methane dissolves away is shown in detail in Figure 8. The top panel reports the bubble density as a function of time for the experiment depicted in Figure 7. Both

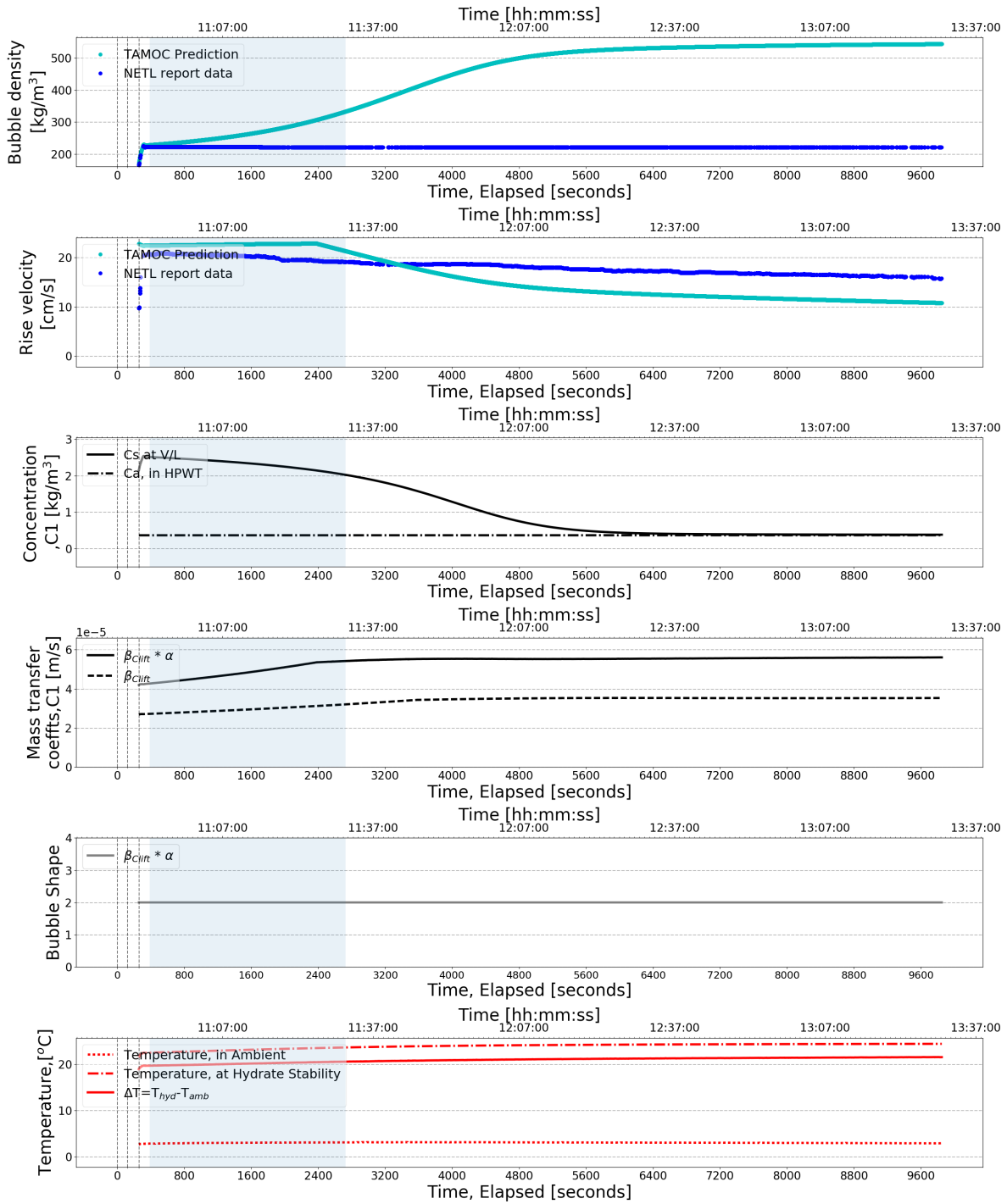


Figure 8: Bubble properties as a function of time for the natural gas bubble (C1C2C3) presented in Figure 7. Bubble density and rise velocity are computed in TAMOC using the mixture equation of state and tracking the evolving mixture as the bubble dissolves. Equivalent parameters are computed in the NETL report data assuming a constant bubble composition.

TAMOC and the Levine et al. (2015) report start at the same bubble density. Methane rapidly begins to dissolve, and the bubble in the TAMOC simulation becomes more dense. Much of the dissolution concludes after about 6,400 s, after which the TAMOC prediction for the density also plateaus. The difference between the TAMOC and Levine et al. (2015) densities is about a factor of two in this late stage of the experiment. Rise velocity is much less affected, and the TAMOC simulation predicts a slightly lower rise velocity corresponding to the more dense bubbles. Since the difference in rise velocity is small, Levine et al. (2015) could not observe the density increase of the bubbles purely by monitoring the water tunnel downdraft speed.

Since bubble size is the quantity actually observed in the experiments, this is the correct variable to use to validate the model, and Figure 7 shows that TAMOC does a very good job predicting the bubble size in the natural gas mixture experiment. These simulations further confirm that the bubble composition changes enough over the course of the experiment that a constant bubble composition cannot be assumed. Hence, the mass versus time plots presented in Levine et al. (2015) are biased toward lower than actual mass in cases where gas mixtures were used in the experiments.

Cases with Hydrate Formation. The validation cases above without a hydrate shell use the values of the mass transfer amplification factor α calibrated from the same experiments; hence, they show the sensitivity of the model to α but do not rigorously validate the model performance. On the other hand, cases with a hydrate shell that were not used in selection of the calibrated α will yield a true model validation. This exercise is reported here.

Figure 9 shows the measured mass reduction rates compared to the theoretical rates in TAMOC, using a similar format to the figures above without hydrate, but with different symbols and a color bar now presenting a temperature difference instead of a pressure ratio. As expected for a validation case, there is greater scatter in the data. For points that lie above the 45° line, we explained in our previous quarterly report that the equation of state in TAMOC predicts a slightly higher solubility of methane than the true equation of state. When the background dissolved gas concentration is high, this retards the dissolution of the bubble in the model, and for the light-colored points in the second quadrant of the plot, bubbles grow in the experiments while TAMOC predicts them to shrink. This only becomes a problem when the dissolved background concentration C is close to solubility C_s so that the difference $(C - C_s)$ approaches zero. This disagreement is acceptable since the background dissolved methane concentration will rarely be high in the ocean, and the 5%

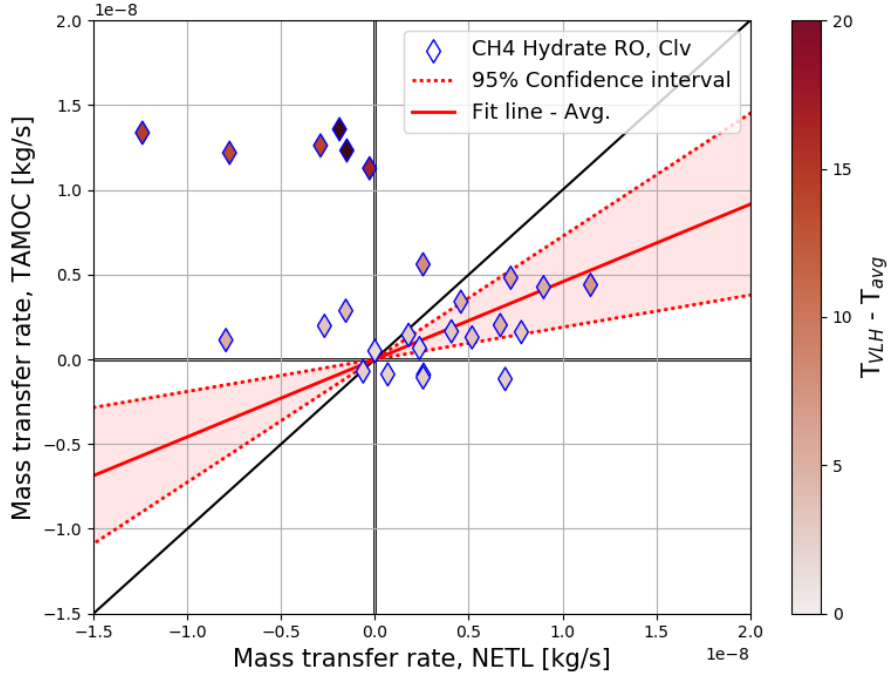


Figure 9: Comparison of observed and modeled mass transfer rate dm/dt for pure methane bubbles in RO water with a hydrate skin.

error in the solubility using the TAMOC equation will always be a small contribution to the total driving force ($C - C_s$) when C approaches zero background concentration.

Several other points in Figure 9 require more careful consideration. These are the points with negative x -axis values and that lie above 1.0 on the y -axis. All of these points are at hydrate subcooling values $T_{hyd} = (T_{VLH} - T)$ greater than 10°C , where T is the ambient temperature and T_{VLH} is the temperature at the vapor-liquid-hydrate equilibrium point. In these cases, the hydrate shell becomes thicker, and the free gas can no longer escape from the bubble into the water column directly through cracks in the hydrate shell. Then, the main source of dissolution becomes hydrate. As a result, we use the solubility of hydrate as the correct value in the mass transfer equations in TAMOC whenever T_{hyd} exceeds 10°C .

For experiments with hydrates at lower pressure where $T_{hyd} < 10^\circ\text{C}$, we use the same mass transfer model as in the no-hydrate cases above (i.e., dirty-bubble mass transfer rates with the free gas dissolving). Figure 10 shows an example case for a pure methane bubble with a hydrate skin. The system pressure is maintained constant throughout each period of the figure shaded in light blue, and because the hydrate subcooling is not too great, the free gas inside the bubble can still escape, and the model works well using C_s for methane gas in the mass-transfer calculation.

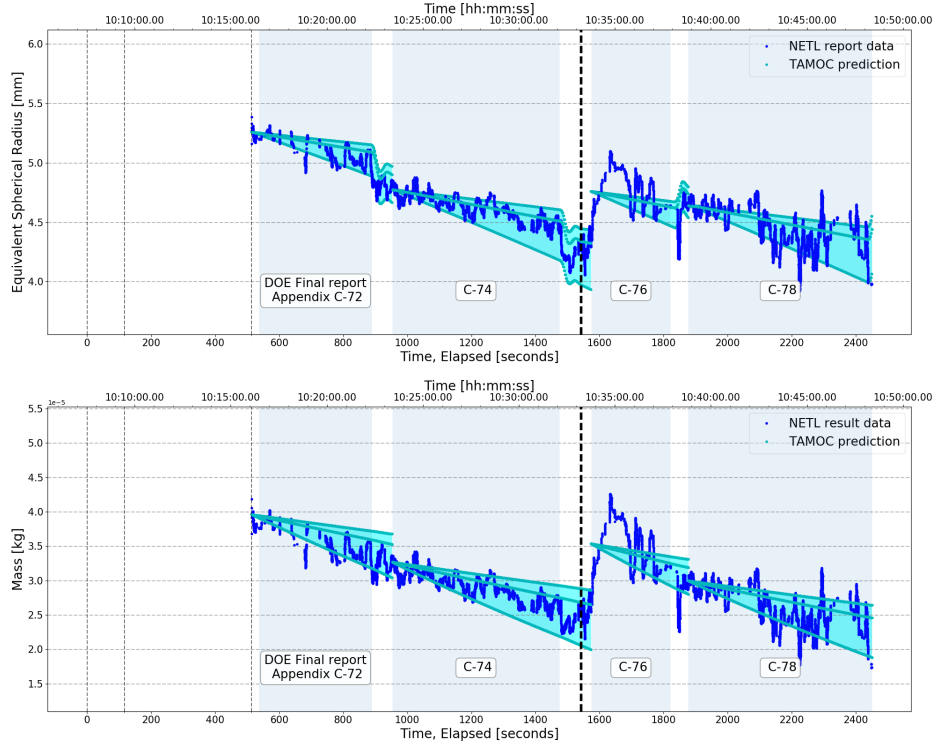


Figure 10: Comparison of TAMOC model simulations with the measured data. Upper panel: equivalent spherical radius; lower panel: bubble mass. Results for a pure methane bubble in RO water with a hydrate skin at $T_{hyd} < 10^{\circ}\text{C}$.

At higher sub-cooling, we can also use C_s for methane gas when the system pressure is continuously changing. Note, such cases are not plotted in Figure 9 since a mean bubble shrinkage rate in these experiments combines the effects of dissolution and pressure expansion; such cases can only be evaluated using TAMOC and a variable background pressure as a function of time. Figure 11 shows an example of pure methane bubbles with a hydrate shell under variable pressure conditions. In the upper panel of the figure, the system pressure never exceeds a hydrate subcooling greater than about 2°C , and we would expect the free gas to be dissolving. In the lower panel, for times after 1,300 s, the system pressure exceeded conditions for a subcooling above 10°C . We simulated the complete case using the solubility of the free gas based on the hypothesis that the rapid size changes caused by the changing pressure helps to maintain cracks in the hydrate skin that allow free gas to escape. In both cases, the normal model with dirty bubble mass transfer and using C_s for methane gas tracks the experimental results fairly well.

When the system pressure remains constant at a high subcooling ($T_{hyd} > 10^{\circ}\text{C}$), then the bubbles do not shrink at a rate consistent with dissolution of the free gas inside the bubble. Instead,

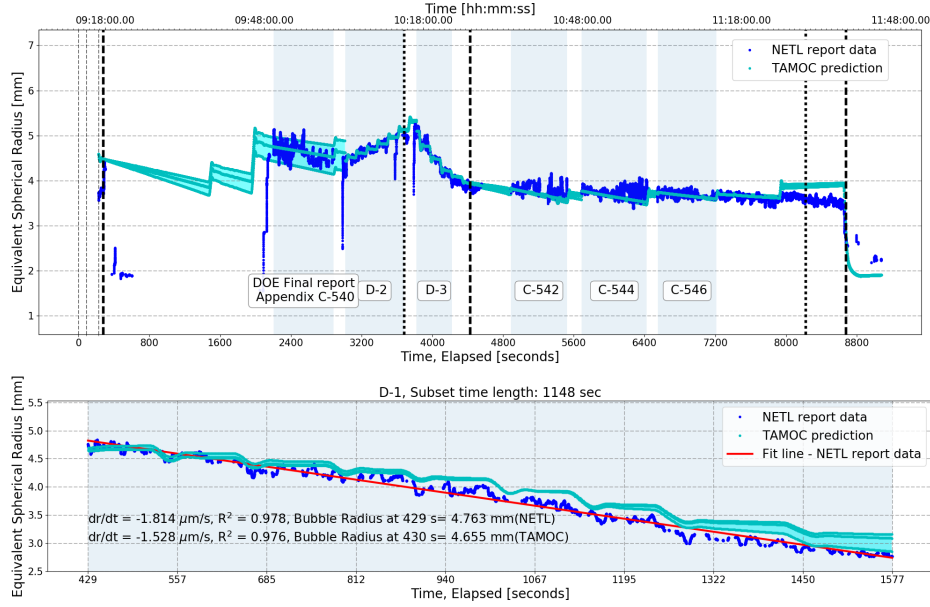


Figure 11: Comparison of TAMOC model simulations with the measured data: equivalent spherical radius. Results for a pure methane bubble in RO water for an experiment with variable system pressure. Upper panel: low pressure experiment; lower panel: high-pressure experiment.

the hydrate skin appears thicker, and dissolution becomes consistent with dissolution of the hydrate shell. Figure 12 shows an example. In such cases, we use the solubility C_s of the hydrate

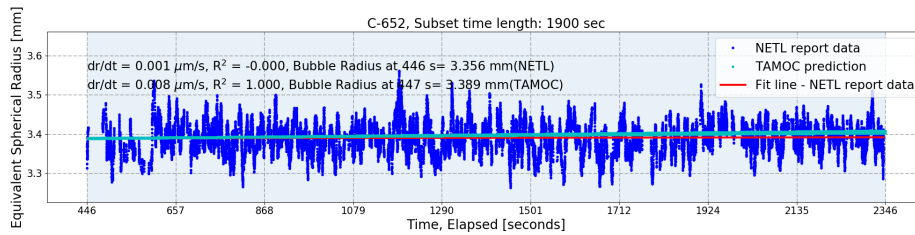


Figure 12: Comparison of TAMOC model simulations with the measured data: equivalent spherical radius. Results for a pure methane bubble in RO water for an experiment with constant pressure at $T_{hyd} > 10^\circ\text{C}$. Modeled using C_s of hydrate instead of free gas.

phase instead of the free gas phase to set the chemical potential in the dissolution equation. This results in much slower dissolution and in results that match the measured data, as seen in the figure.

Summary and Conclusions. In summary, we have used the entire database of NETL HPWT data to calibrate and validate our model for dissolution of methane bubbles at high pressure with and without a hydrate shell. We calibrated the model by comparing theoretical mass transfer rates dm/dt for bubbles in quiescent ambient water to rates measured in the HPWT. In all cases,

dirty bubble mass transfer rates agreed best with the measured data and rates observed in the HPWT were about 1.6 times larger than theoretical values in quiescent water. This mass transfer amplification factor α was then selected by comparing to experiments without a hydrate shell, and Table 1 summarizes the mean value and values spanning a 95% confidence interval.

Using this calibrated parameter α , we then simulated the time-varying bubble size for each NETL experiment, both with and without hydrate skins. The figures above document typical cases. For cases without a hydrate skin, the model tracks the measured bubble sizes very well. When the injected gas is a mixture of C1C2C3, the model also predicts the correct measured bubble sizes and demonstrates that estimates of the evolution of the bubble mass based on a constant gas composition are biased toward lower masses than occurred in the water tunnel since the bubble tends to become more dense as the more-soluble methane dissolves preferentially from the bubbles. In cases with a hydrate skin, dirty bubble mass transfer rates and a driving mass transfer concentration gradient given by the solubility C_s of pure gas work in cases for low hydrate subcooling ($T_{hyd} < 10^\circ\text{C}$) and when the system pressure is changing. When higher subcooling occurs at a constant system pressure, the mass transfer is better described by dissolution of the hydrate and modeled using C_s for the hydrate instead of the pure gas. A complete data archive containing all model simulation data, the model source code, and plots of the results of each experiment following the format of the plots contained here is provided as the deliverable for Milestone 5: Quantify seep model performance.

Subtask 4.2 - Validate to GISR Field Data.

In the GISR field experiments, three observation platforms were used: *in situ* imaging from the stereoscopic imaging system at discrete points from the sea floor to about 250 m altitude and acoustic backscatter measurements from the EM 302 haul-mounted multibeam sonar and from the M3 multibeam sonar mounted on the ROV. In this Subtask, we validate the TAMOC model predictions at the seeps surveyed during the G07 and G08 GISR expeditions to these measured data.

For the GISR data, the raw data are camera images and acoustic backscatter. These data can be post-processed to yield the following types of observations for model validation:

1. Bubble Size Distribution and Flow Rate. The cameras mounted on the ROV provide measurements of the bubble sizes and their flow rates. At the sea floor, these are used as initial

conditions to the model and do not represent validation data. At various heights above the sea floor, these data were collected at a small region within a much larger bubble column. These data for bubble size distribution may be used to ground-truth the model simulations, but because of their localized nature, they are more useful to calibrate the acoustic images (Subtasks 5 and 6) than to validate the TAMOC simulations.

2. The EM 302 Watercolumn Backscatter. The haul-mounted EM-302 provides vertical profiles of the seep flare hydro-acoustic signals. Here, we use the observed height of maximum bubble rise in the acoustic data and compare this to the predicted rise heights of these natural seeps in TAMOC. In Subtask 6, we further compare the acoustic backscatter intensity to the bubble flow rate using the validated model.
3. ROV Cross-sections of M3 Backscatter. ROV acoustic images show the cross-sectional profiles of the bubble flares at different heights. These data are used to validate the transport characteristics of the bubbles in TAMOC (lateral and streamwise spreading). This is accomplished by comparing the acoustic cross-section images to the predicted bubble distributions in TAMOC for the same locations.

Together, these data validate the dissolution rate (largely through Item 2) and turbulent spreading (largely through Item 3) predicted by TAMOC for the natural seeps observed during the GISR field cruises.

Validation to Camera Bubble Size Data. For TAMOC simulations of the GISR natural seep data, the bubble size distribution at the seafloor is provided as an initial condition to the model. These data were measured *in situ* by our camera system, and we simulate these seep flares by generating a random sample of bubbles that match the measured size distribution at the source and measured gas flow rate. As the bubbles rise through the water column, they dissolve and shrink. Camera measurements were made at several elevations between the seafloor and an altitude of about 150 m above the source. As the bubbles rise, they also spread out, and the camera sample volume no longer contains all of the bubbles. Instead, it contains a truncated size distribution of bubbles in one part of the plume. This makes it challenging to compare model simulations to the measured data.

Since the measured size distributions at height above the seabed are truncated, they are not appropriate for use in model validation. They can ground-truth the model in the sense that the

model should predict bubble sizes within the measured range. However, since we initialize the model with the measured size distributions and the measurements are made close to the seafloor, this is not a difficult test for the model, and the model performs well.

The best use of the bubble size distribution measurements is to calibrate the M3 data (which we have done in Task 3, above). After the OTRC experiments, we will use the calibrated M3 data to obtain much better quantification of bubble sizes at all heights in the bubble flares. This will be used in Task 6 as we apply the model to simulate the GISR seep flares. As for Subtask 4.2, the bubble sizes observed by the camera only weakly test the model, and the model performed well.

Validation to EM 302 Water Column Data. In our previous quarterly reports, we presented a detailed validation of the TAMOC model predictions to the EM 302 water column data. For that validation, we used a mass transfer correction factor of $\alpha = 1$, appropriate for natural seep bubbles transiting through the nearly quiescent ocean water column (vertical velocities in the oceans are negligible).

We tested three main hypotheses for comparing the predicted seep heights to heights observed in the EM 302 data. These hypotheses determine how the acoustic data are interpreted, and were:

1. The water column backscatter is the sum of the acoustic target strength within the sample volume of the multibeam, and the bubble flare will disappear when the target strength falls below the ambient noise and measurement resolution of the multibeam. This idea is similar to the work currently being conducted by Tom Weber and being applied to split-beam acoustic data. In this hypothesis, all bubbles exiting the sea floor combine to predict the flare rise height.
2. The bubbles spread out enough that the multibeam will sense the bubble plume as long as one bubble has a target strength large enough to be above the noise level of the instrument. In this case, the largest bubbles exiting the sea floor will predict the flare rise height.
3. The flare will remain observable as long as a certain percentage of the initial gas flow rate is still present in the bubble flare. Like case 1, all bubbles exiting the sea floor combine to predict the flare rise height, but it is the bubble mass and not their acoustic backscatter that sets the criterion for being observable.

Through our model validation exercise, we determined that hypothesis 2 is the most physically

intuitive method that requires the least input data, and the model performs very well using this method. Our previous quarterly reports showed that using d_{98} as the bubble size for prediction of the flare height, we have an r^2 value of 0.98, comparing our model-predicted flare rise heights to the measured data, a bias of 41 m absolute height (out of rise heights between 400 m and 1800 m), and an average mean percentage error of rise height of 4.7%. This level of performance over this diverse set of experiments is quite good. Hence, we conclude that our model for predicting flare height validates adequately to the haul-mounted EM-302 dataset.

Validation to M3 Cross-section Profiles. In our previous quarterly report, we presented comparison of the TAMOC prediction between the M3 acoustic data and the model. The agreements were very good, and we accepted the model performance. Hence, the TAMOC model is considered to be validated to the available acoustic data from the GISR expeditions.

Subtask 4.3 - Finalize and Distribute Seep Model. As of the present reporting period, we have concluded our calibration and validation of the seep model. We provide the source code of the model with the archive of NETL HPWT simulation results. The model is also maintained as publicly available through the Github code sharing website (see Section 2 Products, below). This concludes the major activity under Task 4.

Progress Toward Milestone Milestone 4 (Adapt TAMOC model to NETL data) was completed on June 19, 2018. As of this report, we have also concluded the work required for Milestone 5 (Quantify seep model performance). We have summarized the seep model performance in this and recent quarterly reports and have prepared a complete data archive of model results to be transferred to NETL.

1.3 Decision Point 2

The report for Decision Point 2 was completed and submitted as of May 31, 2018. Based on successful completion of the go/no go success criteria for Decision Point 2 outlined in the PMP, we were granted permission to continue into Task 5 (OTRC Experiment).

1.3.1 Task 5.0: Conduct No-Hydrate M3 Calibration Experiment in OTRC

In our original project timeline (Figure 1), the OTRC experiment was scheduled for the third quarter of Phase 2. Through discussions with the Project Manager, we elected to delay this experiment to the first quarter of Phase 3 in order that we can combine this experiment with a similar experiment funded through another project. In that project, the Co-PI Binbin Wang is developing an *in situ* measurement platform for particle image velocimetry, which will allow us to measure water velocity within the bubble column during our experiments. This is important to quantify possible upward velocities of water that have been hypothesized in the literature to be as large as 10% of the bubble rise velocity. Unfortunately, the filter pump that serves the OTRC wave basin broke shortly before we were scheduled to conduct the experiments, and operations at the OTRC were postponed during pump repairs. Since then, the pump has been repaired and the OTRC has resumed operations. We are now scheduled to conduct our OTRC experiments on February 25-28, 2019. This delay does delay the start of Subtask 6.1, but we have been busy completing Task 4 and working on other subtasks so that this delay has not delayed completion of the overall project.

1.3.2 Task 6.0: Apply Seep Model to GISR Multibeam Echosounder Data

In this Task, we use the seep model developed in Task 4 together with the acoustic data analyzed in Task 2 and refined in Task 5 to evaluate the characteristics of the natural seeps at MC 118 and GC 600. This includes an evaluation of the acoustic signature of hydrate shells that may be present in the M3 acoustic cross-sectional data obtained by the ROV and the water column trajectory and flow rate that may be extractable from the haul-mounted EM 302. Together, these activities will explore the role of hydrate shells on the fate of methane from natural seeps and predict the vertical distribution of methane in the water column originating from these seep sources.

Subtask 6.1 - Analyze M3 Data to Characterize Hydrate Shells. We will continue this Subtask following completion of Task 5. We have already developed acoustic models of the M3 data (Milestone 3) and have achieved favorable comparison between the TAMOC simulations and the M3 acoustic images (Subtask 4.2). Hence, this work is well underway and will be concluded quickly once the OTRC experiments are analyzed.

Subtask 6.2 - Analyze EM-302 Data for Bubble Concentration. In this Subtask, we will

use the TAMOC model together with the EM 302 acoustic data to obtain predictions of the gas flow rate as a function of height above each seep observed in the GISR field experiments. In the quarterly report for Phase 2, Quarter 3, we showed our first step of comparing the trajectories predicted by the TAMOC model with those observed in the EM 302 data. In the quarterly report for Phase 2, Quarter 4, we also classified all of the acoustic data from the EM-302 GISR dataset for this subtask. During the present reporting period we have set up the model to run each case but have not yet generated reportable results. Instead, we focused on Tasks 4 and 7.

1.3.3 Task 7.0: Document Model Validation

In this Task, we document the model validation through reporting to NETL, distribution of the model over Github, and reporting of our findings in journal articles in the peer-reviewed literature.

During the present reporting period, we have concluded the model validation outlined in Task 4, which includes validation to both the NETL HPWT dataset and the GISR field observations. We have begun drafting these results in the form of journal manuscripts. One manuscript is already largely completed and will report on the GISR observations from Task 3 above; this manuscript is intended for submission to *Geophysical Research Letters*. We have also drafted a manuscript reporting on our mass transfer models and hydrate formation time, including validation to the GISR EM-302 rise height data. This work will likely be submitted as two manuscripts to different geophysics journals. Finally, we are beginning to write up our progress comparing to the NETL HPWT data. As this is the most recent work we have concluded, this manuscript is in an early stage. Each of these manuscripts will be a major portion of our project effort continuing into the remainder of project Phase 3.

1.4 Deliverables

To date, we have completed the following list of deliverables:

1. **Project Management Plan (PMP)**. The PMP was delivered in its accepted and final form on October 28, 2016.
2. **Data Management Plan (DMP)**. No revisions were requested by the Project Officer to the plan submitted with the proposal; hence, the original DMP is the present guiding document. Revisions will be updated as necessary throughout the project as required by the Project Officer.

3. **Task 2 NETL HPWT Analyzed Data.** The recipient shall provide time series of hydrate formation time, periods of crystal motion on the bubble/water interface, and bubble equivalent spherical diameter to NETL in the format of their choice (ASCII, Matlab, NetCDF, etc.) by the end of Task 2. We have provided these data through the reports for Milestone 2, Decision Point 1, and the quarterly reports.
4. **Task 3 GISR Seep Cruise Analyzed Data.** The recipient shall provide all post-processed analyses of the GISR high-speed camera data for the Gulf of Mexico seep cruises along with time series of corresponding M3 and EM-302 datasets. The camera data shall be provided to NETL in the format of their choice; M3 and EM-302 data shall be provided in the manufacturer raw format. The recipient shall submit these data to NETL by the end of Task 3. We have provided these data through the reports for Milestone 3, Decision Point 1, and the quarterly reports.
5. **Task 4 Validated Seep Model.** The recipient shall provide the refined and validated seep model to NETL. The recipient shall submit the model to NETL by the end of Task 4. We have provided the source code to the validated seep model in the data archive submitted for Milestone 5, Quantify seep model performance.

As of the present reporting period, we have concluded the deliverables for Tasks 2, 3, and 4. The next set of deliverables will summarize the results of the OTRC acoustic experiment (Task 5). Progress toward these deliverables is summarized above in the reporting for each Task.

1.5 Milestones Log

Table 2 presents the schedule of milestones with their verification methods for the duration of the project period. Milestones 1 through 5 were completed on time. See Section 1.2 for details on progress toward completion of up-coming milestones. The Table reflects the change to the project schedule such that the OTRC experiment (Task 5) will be conducted in February 2019, with the Milestone report now due in March 2019. All other Milestones are proceeding as planned in the Project Management Plan.

1.6 Plans for the Next Reporting Period

During the next reporting period, we will be focused on conducting the OTRC experiment (Task 5) and applying the validated seep model to simulate the acoustic data collected through the GISR

Table 2: Milestones schedule and verification methods.

	Milestone	Comments
Title	Acquisition of NETL HPWT data	
Date Completed	March 24, 2017	
Verification Method	Email verification	
Title	Adapt Matlab code to NETL data	
Date Completed	September 28, 2017	
Verification Method	Report	
Title	Matlab code for M3 and EM-302 data	
Date Completed	September 29, 2017	
Verification Method	Report	
Title	Adapt seep model to NETL data	
Date Completed	June 19, 2018	
Verification Method	Report	
Title	Quantify seep model performance	
Date Completed	January 31, 2019	
Verification Method	Quarterly Reports and Data Archive	
Title	OTRC Experimental Report	
Planned Date	March 2019	
Verification Method	Report	
Title	Quantify performance of acoustic models	
Planned Date	March 2019	
Verification Method	Report	

cruises (Task 6). We have also begun writing journal papers to summarize the results of this project (Task 7). Drafts of these papers will be provided as they are submitted to journals, beginning in the 2nd Quarter of Budget Period 3.

For Task 5, we are scheduled to use the OTRC from February 25-28, 2019. We will analyze the data immediately and prepare the experiment report for submission in March 2019. Although this is later than planned and has delayed progress on Subtask 6.1 (Analyze GISR M3 data), with the planned no-cost extension (see Section refsec:changes), this delay will not impact our ability to complete all tasks by the end of the project.

For Task 6, we will focus on analyzing bubble concentration using the EM-302 data. Much of this work has been completed, and we are in the stages now of quantifying the model performance and drafting a journal article to report our findings.

References

- Clift, R., J. R. Grace, and M. E. Weber (1978), *Bubbles, drops, and particles*, Academic Press.
- Gros, J., C. M. Reddy, R. K. Nelson, S. A. Socolofsky, and J. S. Arey (2016), Simulating GasLiquidWater Partitioning and Fluid Properties of Petroleum under Pressure: Implications for Deep-Sea Blowouts, *Environ Sci Technol*, 50(14), 7397-7408.
- Medwin, H. and C. S. Clay (1998), *Fundamentals of Acoustical Oceanography*, Academic Press, Boston, 712 pp.
- Levine, J., I. Haljasmaa, R. Lynn, F. Shaffer, and R. P. Warzinski (2015), Detection of Hydrates on Gas Bubbles during a Subsea Oil/Gas Leak, NETL-TRS-6-2016, EPAAct Technical Report Series, U.S. Department of Energy, National Energy Technology Laboratory: Pittsburgh, PA.
- Rehder, G., I. Leifer, P. G. Brewer, G. Friederich, and E. T. Peltzer (2009), Controls on methane bubble dissolution inside and outside the hydrate stability field from open ocean field experiments and numerical modeling, *Marine Chemistry*, 114(1-2), 19–30.
- Römer, M., H. Sahling, T. Pape, G. Bohrmann, and V. Spiess (2012), Quantification of gas bubble emissions from submarine hydrocarbon seeps at the Makran continental margin (offshore Pakistan), *J Geophys Res-Oceans*, 117(19), 2011jc007424.
- Warzinski, R. P., F. Shaffer, R. Lynn, I. Haljasmaa, M. Schellhaas, B. J. Anderson, S. Velaga, I. Leifer, and J. Levine (2014a), The role of gas hydrates during the release and transport of well fluids in the deep ocean, DOI/BSEE Contract E12PG00051/M11PPG00053, Final Report, U.S. Department of Energy, National Energy Technology Laboratory.
- Warzinski, R. P., Lynn, R., Haljasmaa, I., Leifer, I., Shaffer, F., Anderson, B. J., and Levine, J. S. (2014b). Dynamic morphology of gas hydrate on a methane bubble in water: Observations and new insights for hydrate film models. *Geophys Res Lett*, 41(19), 2014GL061665.
- Weber, T. C., L. Mayer, K. Jerram, J. Beaudoin, Y. Rzhonov, and D. Lovalvo (2014), Acoustic estimates of methane gas flux from the seabed in a 6000 km(2) region in the northern gulf of mexico, *Geochemistry Geophysics Geosystems*, 15(5), 1911–1925.

2 Products

2.1 Publications, Conference Papers, and Presentations

- Socolofsky, S. A., Kim, B., Kovalchuk, M., Levine, J., and Wang, B., “Mass transfer rates for hydrate-armored bubbles in the NETL High Pressure Water Tunnel,” Poster presented at the Gordon Research Conference on Natural Gas Hydrate Systems, Galveston, Texas, February 25 to March 2, 2018.
- Kim, B., Socolofsky, S. A., and Wang, B., “Hydrate formation time analyzed from data for NETL High Pressure Water Tunnel experiments,” Poster presented at the Gordon Research Conference on Natural Gas Hydrate Systems, Galveston, Texas, February 25 to March 2, 2018.

2.2 Websites or Other Internet Sites

The natural seep model used for this project, the Texas A&M Oilspill Calculator (TAMOC), is published via an open source code sharing service at:

<http://github.com/socolofs/tamoc>

2.3 Technologies or Techniques

Nothing to report.

2.4 Inventions, Patent Applications, and/or Licenses

Nothing to report.

2.5 Other Products

Nothing to report.

3 Participants and other collaborating organizations

3.1 Project Personnel

- 1. **Name:** Scott A. Socolofsky
- 2. **Project Role:** Principal Investigator

- 3. **Nearest person months worked during reporting period:** 1
 - 4. **Contribution to Project:** Overall project management and direction. Dr. Socolofsky has led the collection of the HPWT data, directed the data analysis methods, and completed all project reporting requirements.
 - 5. **Collaborated with individual in foreign country:** No
 - 6. **Travelled to foreign country:** No
- 1. **Name:** Binbin Wang
 - 2. **Project Role:** Co-Principal Investigator
 - 3. **Nearest person months worked during reporting period:** 2
 - 4. **Contribution to Project:** Analyzed the image data for the G08 cruise, created model for acoustic data from M3 sonar and EM-302 multibeam, and compared the measured data to model results from TAMOC. He also trained the Ph.D. student to begin analysis of the NETL HPWT data.
 - 5. **Collaborated with individual in foreign country:** No
 - 6. **Travelled to foreign country:** No
- 1. **Name:** Byungjin Kim
 - 2. **Project Role:** Ph.D. Student
 - 3. **Nearest person months worked during reporting period:** 3
 - 4. **Contribution to Project:** Organized the HPWT data, summarized the existing results from the NETL reports, and analyzed HPWT data for bubble size, hydrate formation time, and bubble interface mobility.
 - 5. **Collaborated with individual in foreign country:** No
 - 6. **Travelled to foreign country:** No
- 1. **Name:** Soobum Bae
 - 2. **Project Role:** Ph.D. Student
 - 3. **Nearest person months worked during reporting period:** 3
 - 4. **Contribution to Project:** Soobum Bae is working as an unfunded Master of Science student to help analyze the HPWT data. He has helped to classify the video image data and to evaluate the hydrate equation of state.

5. **Collaborated with individual in foreign country:** No

6. **Travelled to foreign country:** No

3.2 Partner Organizations

None to report.

3.3 External Collaborators or Contacts

This project works in close collaboration with researchers in the DOE/NETL funded project “Fate of Methane in the Water Column,” led by the U.S. Geological Survey (USGS) in Woods Hole (Carolyn Ruppel), and with a new project led by the University of Rochester (John Kessler) to advance understanding of the environmental implications that methane leaking from dissociating gas hydrates could have on the ocean-atmosphere system. Dr. Socolofsky visits and communicates with researchers in these projects regularly and shares updates on work in progress. Accomplishments associated with these collaborations are detailed in Section 1.

4 Impact

None at this point.

5 Changes / Problems

Personnel. As reported in past quarterly reports, one adjustment from the proposed activities in the PMP is that a Ph.D. student (Byungjin Kim) was not hired to work on this project until the second quarter of project Phase 1, instead of our original plan to hire a student in the first quarter. This occurred as it took time to complete contract negotiations and to effectively recruit a high-quality student to this project. Despite this delay in hiring, the project activities have remained on schedule. We anticipate that this hiring delay will result in the need for a short no-cost extension at the end of the project.

One other change is that we have had to delay the OTRC experiment (Task 5) both to benefit from a parallel effort of the Co-PI and because of closure of the lab during repairs to the filter pump in November through January. This is discussed in detail above in Section 1.3.1. The expected delay for Task 5 is six months, which is similar to the delay outlined above with respect to the

Ph.D. student hiring so that we expect to conclude all planned project tasks by the end of the short, no-cost extension expected above.

6 Special Reporting Requirements

None required.

7 Budgetary Information

Table 3 reports expenditures for Phase 1 of the project, and Table 4 for Phase 2. Table 5 summarizes expenditures for the current phase (Phase 3) of the project.

Table 3: Budget Report for Phase 1

Baseline Reporting Quarter	Budget Period 1							
	Q1		Q2		Q3		Q4	
	10/1/16 - 12/31/16		1/1/17 - 3/31/17		4/1/17 - 6/30/17		7/1/17 - 9/30/17	
DE-FE0028895	Q1	Cumulative Total	Q2	Cumulative Total	Q3	Cumulative Total	Q4	Cumulative Total
Baseline Cost Plan								
Federal Share	\$33,752	\$33,752	\$29,716	\$63,468	\$27,810	\$91,278	\$53,034	\$144,312
Non-Federal Share	\$12,029	\$12,029	\$12,029	\$24,058	\$8,019	\$32,077	\$4,009	\$36,086
Total Planned	\$45,781	\$45,781	\$41,745	\$87,526	\$35,829	\$123,355	\$57,043	\$180,398
Actual Incurred Cost								
Federal Share	\$11,037	\$11,037	\$22,617	\$33,654	\$25,957	\$ 59,610	\$ 69,499	\$129,110
Non-Federal Share	\$12,029	\$12,029	\$12,029	\$24,058	\$8,019	\$32,077	\$4,009	\$36,086
Total Incurred Costs	\$23,066	\$23,066	\$34,646	\$57,712	\$33,976	\$91,687	\$73,508	\$165,196
Variance								
Federal Share	\$-22,715	\$-22,715	\$-7,099	\$-29,814	\$-1,853	\$-31,668	\$16,465	\$-15,202
Non-Federal Share	\$0	\$0	\$0	\$0	\$0	\$0	\$0	\$0
Total Variance	\$-22,715	\$-22,715	\$-7,099	\$-29,814	\$-1,853	\$-31,668	\$16,465	\$-15,202

Table 4: Budget Report for Phase 2

Baseline Reporting Quarter	Budget Period 1							
	Q1		Q2		Q3		Q4	
	10/1/16 - 12/31/16		1/1/17 - 3/31/17		4/1/17 - 6/30/17		7/1/17 - 9/30/17	
DE-FE0028895	Q1	Cumulative Total	Q2	Cumulative Total	Q3	Cumulative Total	Q4	Cumulative Total
Baseline Cost Plan								
Federal Share	\$18,473	\$162,785	\$35,552	\$198,337	\$22,681	\$221,018	\$44,423	\$265,441
Non-Federal Share	\$10,125	\$46,221	\$10,125	\$56,336	\$6,750	\$ 63,086	\$ 3,374	\$66,460
Total Planned	\$28,598	\$208,996	\$45,677	\$254,673	\$29,431	\$ 284,104	\$47,797	\$331,901
Actual Incurred Cost								
Federal Share	\$29,427	\$158,537	\$29,427	\$187,964	\$28,798	\$216,762	\$16,441	\$233,204
Non-Federal Share	\$10,125	\$46,211	\$10,125	\$56,336	\$6,750	\$ 63,086	\$3,374	\$66,460
Total Incurred Costs	\$39,552	\$204,748	\$39,552	\$244,300	\$35,548	\$279,848	\$19,815	\$299,664
Variance								
Federal Share	\$10,954	\$-4,248.13	\$-6,125	\$-10,373	\$6,117	\$-4,256	\$-27,982	\$-32,238
Non-Federal Share	\$0	\$0	\$0	\$0	\$0	\$0	\$0	\$0
Total Variance	\$10,954	\$-4,248	\$-6,125.64	\$-10,373	\$6,117	\$-4,256	\$-27,982	\$-32,237

Table 5: Budget Report for Phase 3

Baseline Reporting Quarter	Budget Period 1							
	Q1		Q2		Q3		Q4	
	10/1/16 - 12/31/16		1/1/17 - 3/31/17		4/1/17 - 6/30/17		7/1/17 - 9/30/17	
DE-FE0028895	Q1	Cumulative Total	Q2	Cumulative Total	Q3	Cumulative Total	Q4	Cumulative Total
Baseline Cost Plan								
Federal Share	\$14,625	\$280,066	\$14,628	\$294,694	\$23,288	\$317,982	\$43,553	\$361,535
Non-Federal Share	\$8,012	\$74,472	\$8,012	\$82,484	\$5,342	\$87,826	\$2,671	\$90,497
Total Planned	\$22,637	\$354,538	\$22,640	\$377,178	\$28,630	\$405,808	\$46,224	\$452,032
Actual Incurred Cost								
Federal Share	\$13,668	\$246,872	\$	\$	\$	\$	\$	\$
Non-Federal Share	\$8,012	\$74,472	\$	\$	\$	\$	\$	\$
Total Incurred Costs	\$21,680	\$321,344	\$	\$	\$	\$	\$	\$
Variance								
Federal Share	\$-957	\$-33,194	\$	\$	\$	\$	\$	\$
Non-Federal Share	\$0	\$0	\$	\$	\$	\$	\$	\$
Total Variance	\$-957	\$-33,194	\$	\$	\$	\$	\$	\$

National Energy Technology Laboratory

626 Cochran Mill Road
P.O. Box 10940
Pittsburgh, PA 15236-0940

3610 Collins Ferry Road
P.O. Box 880
Morgantown, WV 26507-0880

13131 Dairy Ashford Road, Suite 225
Sugar Land, TX 77478

1450 Queen Avenue SW
Albany, OR 97321-2198

Arctic Energy Office
420 L Street, Suite 305
Anchorage, AK 99501

Visit the NETL website at:
www.netl.doe.gov

Customer Service Line:
1-800-553-7681



U.S. DEPARTMENT OF
ENERGY

**NATIONAL ENERGY
TECHNOLOGY LABORATORY**